Available online at www.sciencedirect.com
SCIENCE DIRECT
Journal of Colloid and Interface Science 300 (2006) 270–278
JOURNAL OF Colloid and Interface Science
www.elsevier.com/locate/jcis

Mesoporous silica–titania composed materials

Paula V. Messina, Marcela A. Morini, María B. Sierra, Pablo C. Schulz *

Colloid and Surface Science Group, Departamento de Química, Universidad Nacional del Sur, Bahía Blanca, Argentina

Received 8 July 2005; accepted 16 March 2006

Available online 24 March 2006

Abstract

Titania mesosized particles were obtained by $TiCl_4$ hydrolysis in Aerosol OT/water/*n*-hexane microemulsion. These particles were incorporated in surfactant templated silica mesoporous materials of MCM-41 and MCM-50 structures. Results depended on the surfactant: hexadecyltrimethylammonium bromide templated materials retained the honeycomb structure with small modifications in their characteristics. The dodecyltrimethylammonium bromide templated material changed from honeycomb to lamellar structure when the titania particles were included, with dramatic changes in the structure characteristics. The didodecyldimethylammonium bromide templated lamellar structure was retained after TIO_2 inclusion, with a slight increase in the specific area, pore diameter and pore walls thickness.

Keywords: Mesoporous material; Silica–titania material; Inverse microemulsion templated particles

1. Introduction

The synthesis of nanoparticles and nanoporous materials is a recent branch of the nanotechnology. The high specific areas obtained, together with the effect of confinement, give rise to nanostructures having properties which differ from those shown by the conventional materials.

A large variety of methods have been proposed to synthesize nanoparticles, among them the use of microemulsions enables the control of particle size.

The inclusion of titania in a mesoporous system is desired because of the catalytic activity of this substance. Anatase is a tetrahedrical crystalline form of titania having high catalytic activity [1]. Anatase is usually formed at low temperatures and preferred for processing microelectronic devices, while rutile, which is also a tetrahedric crystalline form of TiO_2, is formed at relatively high temperatures. There is a rhombic crystalline form of titania, called brookite. Titania has the potential of photooxidation of harmful organic pollutants in wastewater, and the use of TiO_2 heterogeneous photocatalysis for treatment of wastewater and polluted air is one of the most extensively studied processes in recent years [2]. Moreover, TiO_2 is inexpensive, nontoxic and water stable, which makes it amenable for use in a wide range of processes with minimal environmental impact.

The inclusion of titania in silica structures is reported in several works. As examples, Widenmeyer et al. [3] grafted metaloorganic titanium reagents onto dehydrated MCM-48 samples in dry hexane; Xiao et al. [4] produced mesoporous titanosilicates with high catalytic activity; Ogawa [5] produced nanoporous silica films containing titanium; Mrowiec-Bialon [6] synthesized titania–silica aerogels.

The goal of this work is to produce titania nanoparticles hydrophobized by coverage with a monolayer of surfactant, and then to include these particles into the hydrophobic structure of surfactant liquid crystals, which in turn are used to produce silica mesoporous materials. Then the titania nanoparticles will presumably be situated inside the cylindrical pores in honeycomb structures of the MCM-41, or between lamellae in MCM-50 lamellar type materials.

This work is divided in two parts: first, the synthesis of TiO_2 nanoparticles by using an inverse microemulsion composed by *n*-hexane/water/Aerosol OT (AOT). The water microdroplets surrounded by a monolayer of surfactant in a continuous hydrocarbon phase act as micro-reactors to synthesize nanoparticles whose growing is controlled inside the water droplet giving rise to a narrow size distribution.

* Corresponding author.
E-mail address: pschulz@criba.edu.ar (P.C. Schulz).

0021-9797/$ – see front matter
doi:10.1016/j.jcis.2006.03.039

The synthesis of nanoparticles via inverse microemulsions was used previously by many authors. The preparation method using extremely small water pools in reverse micelles as the reaction media has been studied extensively. One of the advantages of this method is that localized supersaturation of the reactants is suppressed and a uniform nucleation occurs, since the reactants are dispersed very well in the reverse micellar solution. In addition, the reverse micelles can protect the nanoparticles against excessive aggregation. As examples, CdS nanoparticles have been prepared in reverse micellar solutions such as AOT/isooctane or AOT/heptane systems [7–11].

The second part deals with the inclusion of these nanoparticles to mesoporous silica structures during the material preparation step. Mesoporous materials were made using tetraethyl orthosilicate (TEOS) in a basic medium. Two hexagonal mesoporous materials were prepared using hexadecyl (= cetyl) trimethylammonium bromide (CTAB) and dodecyltrimethylammonium bromide (DTAB), and one lamellar material by using didodecyldimethylammonium bromide (DDAB) as templates. The inclusion of titania remarkably modified the structure and specific area of the composed materials with respect to the pure silica compounds.

2. Experimental

Sodium dioctyl sulfosuccinate (Aerosol OT, AOT) 99% was from Sigma. The AOT microemulsion was prepared with a water/surfactant ratio $W = 10$. In a flask 1.1276 g AOT and 0.46 g water were weighed, and then the sample was left during 3 h to produce the surfactant hydration. Then 80 mL of *n*-hexane (Carlo Erba, p.a.) were added and the system sonicated to produce the microemulsion. Then 1.4 mL of $TiCl_4$ (Carlo Erba, 99%, $\delta = 1.722\ \mathrm{g\,cm^{-3}}$) were added and left three days to react following the reaction:

$$TiCl_4 + 2H_2O \leftrightarrow TiO_2 + 4HCl. \quad (1)$$

To obtain the TiO_2 nanoparticles the HCl and *n*-hexane were eliminated by evaporation under vacuum. A white compound formed by the titania nanoparticles surrounded by AOT was obtained. Then the material was calcined during 7 h at 540 °C with air flux, and the resulting white powder studied by transmission electron microscopy (TEM).

To obtain the mesoporous material 11.6 mL of TEOS (Aldrich, 99+%) were mixed with 2 mL water and stirred for 10 min at 500 rpm. Then a solution formed by 1.1 g of NaOH in 20 mL water was added drop to drop to the TEOS solution under stirring.

To produce the lamellar mesoporous material a solution of 7.65 g of DDAB in 38 mL water was added 1 min after the addition of the NaOH solution. The resulting gel was stirred for 3 min and then left for 48 h in an autoclave at 100 °C. Then the gel was filtered and washed with distilled water and left to dry at room temperature. Finally it was calcined for 7 h at 540 °C in an air flux.

The silica–titania composed material was prepared by addition of the dry AOT-TiO_2 material obtained without calcination to the solution of DDAB in water and then sonicated to complete suspension of the material. The resulting solution was added to the TEOS + NaOH solution, and the system was treated as that without titania.

To produce the hexagonal mesoporous systems, the DDAB solution was substituted by 38 mL of solution containing 7.62 g of CTAB or 6.44 g DTAB.

Transmission electron microscopy was performed using a JEOL 100 CX II transmission electron microscope, operated at 100 kV with magnification of 100 000×. Observations were made in a bright field. Powdered samples were placed on cooper supports of 2000 mesh.

The nitrogen adsorption isotherms at 77.6 K were measured with a Micrometrics Model ASAPS (Accelerated Surface Area and Porosimetry System) 2020 instrument. Each sample was degassed at 373 K for 720 min at a pressure of 10^{-4} Pa.

To determine the pore radius (R) the Kelvin equation was used [12]:

$$k_B T \ln p_g/p_0 = -2\sigma v \cos\theta / R_m, \quad (2)$$

where k_B is the Boltzmann constant, T the absolute temperature, p_g is the vapor pressure in the gas phase, p_0 is the vapor pressure at saturation onto a flat liquid surface at the temperature T, σ the surface tension of the liquid adsorbate, R_m the mean radius of curvature of the liquid/gas interface, taken as the pore radius, θ the contact radius and v the volume per molecule of liquid adsorbate. For nitrogen at 77.4 K, $\sigma = 8.88$ mN/m, $\theta = 0$ and $v = 0.057589\ \mathrm{nm^3}$ [12]. To determine the Brunauer–Emmet–Teller (BET) area A_{BET}, the nitrogen molecules diameter is taken as 0.43 nm, calculated by assuming the closest packing spheres [13], and the area per molecule $a_m = 0.1620\ \mathrm{nm^2}$ [14].

In the so-called modified Kelvin equation which is the basis of the Barrett–Joyner–Halenda (BJH) method [15], used to extract pore size distribution from the isotherm analysis, $2/R_m$ is replaced by $f/(R - t)$, where R is the pore radius, f the meniscus shape factor, which, provided there is a perfect wetting, equals 1 or 2 in relation to the filling (adsorption) or the empting (desorption) of the pore, and t is the statistical thickness of the adsorption film on a pore wall. The surface layer thickness t for nitrogen adsorption on silica is given by [16]:

$$t\ (\mathrm{nm}) = 0.1\big(13.99/\big(0.034 - \log(p_g/p_0)\big)\big)^{0.5}. \quad (3)$$

From the t-plots proposed by Halsey [17] one can determine the total surface area (A_{ttot}), the external surface area (A_{text}), the pore volume (V_{tp}) and the core volume (V_c), as explained below. The t-plot of pore structure analysis is based on the assumption that micropore filling in porous solids takes place by the formation of successive layers of the adsorbate until the layers in opposite pore walls merge.

3. Results

3.1. TEM photomicrographs

Fig. 1 shows the nanoparticles of TiO_2 obtained after incineration. The average diameter of the particles was $D =$

16.4 ± 0.3 nm, but the size distribution was bimodal with maxima at 13.6 and 18.2 nm (Fig. 2). The structure of the particles seems to be rhombic instead of tetrahedrical. This means that the structure of particles is probably that of brookite, not that of rutile or anatase. The specific area was computed on the basis of the particle size distribution in 90 m^2/g. Zaban et al. [18] synthesized TiO_2 nanoparticles by hydrolysis and pressure treatment of titanium isopropoxide in acidic solutions. The particles were formed by a mixture of anatase and brookite, average size 12.8 nm and surface area 118.5 m^2/g. However, the samples were much more polydisperse than ours, as can be seen in the TEM micrographs in Zaban et al. article.

In literature there are several examples of the influence of the presence of a surfactant in the synthesis system on the structure of the obtained materials. As examples, the presence of additives in aqueous solution of tioacetamide and lead nitrate produces different crystal structures depending on the presence or absence of additives, on the nature of them (poly(methacrylic acid)), CTAB or a mixture of both additives, and on the additive concentration. This phenomenon was explained by the preferential adsorption of the additive on specific crystalline faces, which inhibits the growth of some planes and favors the growth of others [19]; Bujan et al. [20] synthesized calcium hydrogen phosphate dihydrate in the presence of sodium dodecyl sulfate (SDS) and of Aerosol OT (AOT). Below the CMC electrostatic adsorption of surfactant anions on lateral crystal faces inhibited crystal growth and changed crystal morphology. Above the CMC, SDS and AOT caused phase changes: a mixture of calcium hydrogen phosphate dihydrate and octacalcium phosphate was formed; and finally, Lim et al. [21] synthesized hydroxyapatite in water, in aqueous dodecylalcohol with six oxyethylene units (KN6ZA) and in a O/W microemulsion with KN6ZA and petroleum ether and produced different results depending on the nature of the system.

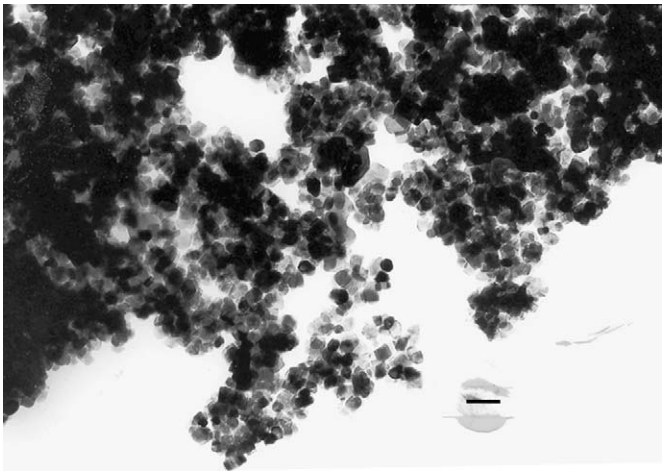

Fig. 1. The TiO_2 particles after calcination of the desiccated colloidal suspension. The bar represents 50 nm.

Normally, the anatase phase of titania is the main product in hydrolytic sol–gel synthesis of nanocrystalline titania. However, brookite (a polytype of anatase) is also typically present in the synthesis product.

The structure of the resulting oxide also depends on the type of precursor: using tetraisopropyl titanate leads to the synthesis of anatase or rutile [22] whereas the use of titanium tetrachloride (as in our case) leads to brookite [23].

Fig. 3a shows the calcined mesoporous material obtained with DTAB, showing the typical array of cylindrical mesopores. The typical honeycomb pore structure with uniform pores of the called MCM-41 can be seen [24–26].

Fig. 3b shows the mesoporous material obtained with DTAB + TiO_2, before calcination. TiO_2 particles included in the system are smaller than those obtained by calcination, with a diameter of about 1.7 nm and remarkably monodisperse.

Fig. 3c shows the calcined mesoporous material obtained with DTAB + TiO_2, showing a more disordered material. The structure seems to be formed by granulated lamellae.

Systems produced with CTAB show the same information, but the honeycomb structure was clearly retained.

Fig. 4a shows the calcined mesoporous material obtained with DDAB, showing lamellae. Fig. 4b shows the calcined mesoporous material obtained with DDAB + TiO_2, showing a more disordered material. Lamellae are present but are smaller

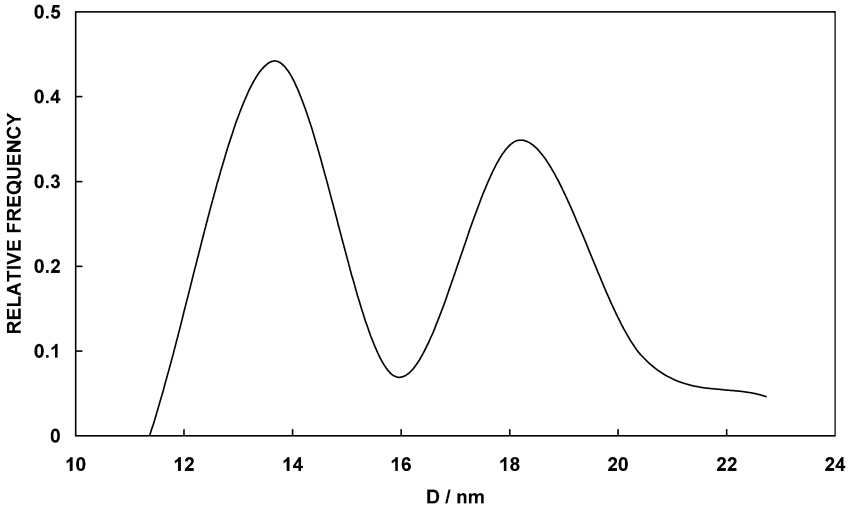

Fig. 2. Size distribution of the titania particles obtained after calcination of the desiccated inverse suspension.

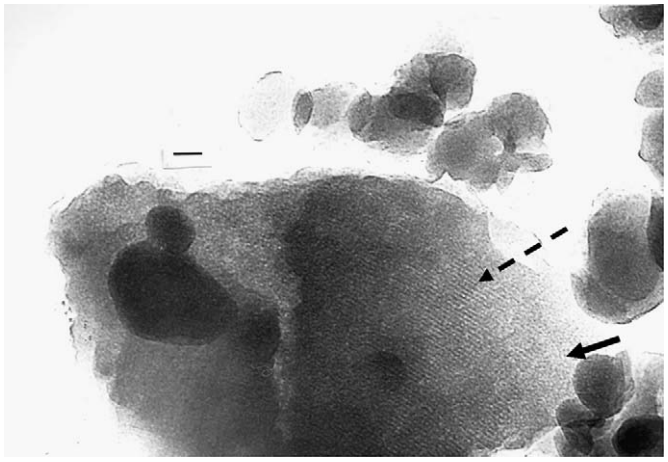

(a)

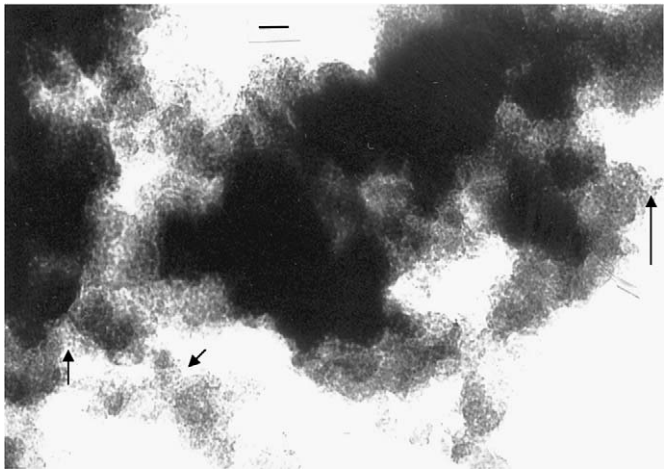

(b)

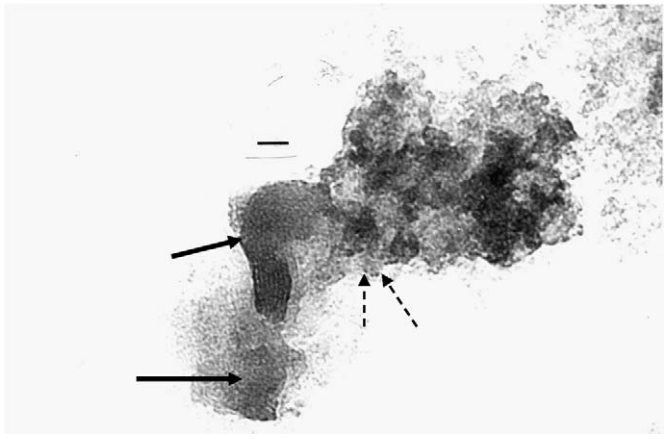

(c)

Fig. 3. (a) The mesoporous material obtained with DTAB (without TiO_2) after calcination. The bar represents 16.75 nm. The dashed arrow indicates the mesopores viewed perpendicular to the pore axes, the full arrow shows the honeycomb structure, i.e., the pores viewed along their axes. (b) The result of the inclusion of the TiO_2 suspension desiccated (but not calcinated) in the system with DTAB. Sample before calcination. The bar represents 16.75 nm. The arrows indicate some of the titania particles. (c) The result of the inclusion of the TiO_2 suspension desiccated (but not calcinated) in the system with DTAB. Sample after calcination. The bar represents 16.75 nm. The dashed arrows show the titania particles, the full arrows show some of the lamellae viewed parallel to their planes.

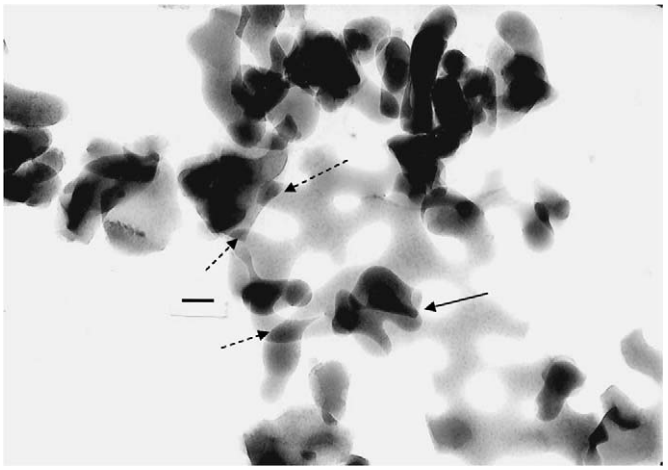

(a)

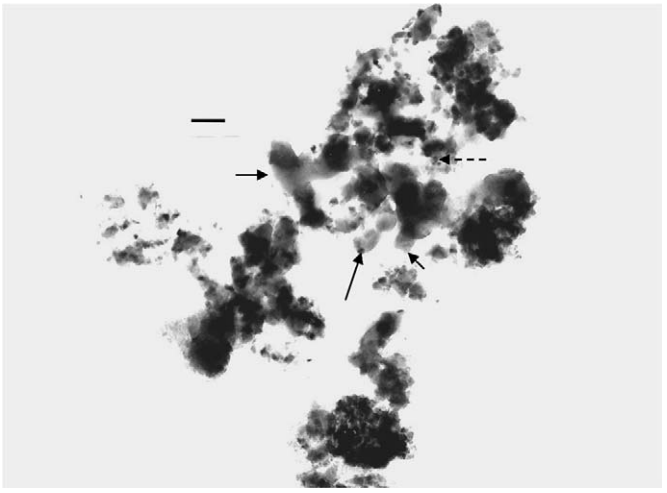

(b)

Fig. 4. (a) Mesoporous material obtained with DDAB after calcination. It may be seen irregular lamellae superimposed. The bar represents 16.75 nm. The full arrow shows three lamellae superimposed, the dashed arrows show two lamellae superimposed. (b) Mesoporous material obtained with DDAB + TiO_2 after calcination. Small irregular lamellae superimposed and some granules (probably titania) may be seen. The bar represents 16.75 nm. The full arrows show small lamellae, the dashed arrow shows three granules of titania.

than in the system without titania. There are granulations with a diameter of 2.9 nm.

Costa Amaral et al. [27] studied AOT/water/*n*-hexane micelles with $[H_2O]/[AOT] = 10$. They found a micelle aggregation number $n = 202 \pm 15$. The size of a titania particle formed by reaction with the $TiCl_4$ and the water in such a reverse micelle may be computed. The number of water molecules in the pool was $10 \times 202 = 2020$. Since each TiO_2 molecule is formed from two water molecules, a micelle gives rise to the formation of 1010 TiO_2 molecules. Using the density of brookite (4.119 ± 0.004 g/cm^3) the volume of the titania particle is 32.50 ± 0.03 nm^3, and assuming spherical shape its diameter is 3.96 ± 0.03 nm. This value is similar to that of the granules observed in the mesoporous materials.

On the other hand, the titania particles obtained by calcination were much larger: 13.6 and 18.2 nm. This may mean that calcination produces synterization of the particles, whilst

the presence of the silica structures produces separation of the original particles and avoids the synterization.

3.2. Nitrogen adsorption

Fig. 5 shows the adsorption/desorption isotherms on the system obtained with CTAB + TiO_2. Typical type IV isotherms showing a hysteresis loop of the type H2 are presented by systems using pure CTAB and DTAB as template, which are characteristic of mesoporous materials [14]. However, the adsorption/desorption isotherm on the system obtained with DTAB + TiO_2 (Fig. 6) is a type II, which is the normal form obtained with non-porous or macroporous adsorbent. It represents unrestricted monolayer–multilayer adsorption. There is a hysteresis of type H4, which is associated with narrow slit-like pores. In the case of slit-like pores, the determined diameter is the pore width.

Fig. 7 shows the related t-plot, and the inset depicts the pore radius distribution of the CTAB + TiO_2. The t-plot shows the typical appearance of material having circularly cylindrical pores [28,29]. A_{ttot} can be calculated from the slope of line A (Fig. 7), while A_{text} can be computed from the slope of line B. The pore surface area was estimated from the difference between A_{ttot} and A_{text}. The pore volume V_{tp} is evaluated from the extrapolating point C, while the core volume V_c is estimated from the length of the vertical line D. Results are shown in Table 1. The systems produced using pure CTAB and pure DTAB as templates are similar. The t-plot or the DTAB + TiO_2 shows the typical appearance presented by adsorbents with slit-shaped pores (Fig. 8). Below point A, no pores are filled; between A and B, mesopores are filled, A indicating the minimum pore size; between B and C, no pores are filled; and above C, Kelvin capillary condensation occurs [28,29]. Since the intercept of the straight line at low t values is not zero, it follows that micropores are also present, whose volume is the intercept, and the slope equals the free surface.

Fig. 9 shows the adsorption/desorption isotherms on the system obtained with pure DDAB and Fig. 10 shows the related t-plot. Fig. 9 is a type II isotherm showing a hysteresis of type H4. Fig. 10 is similar to Fig. 8. Then, both figures indi-

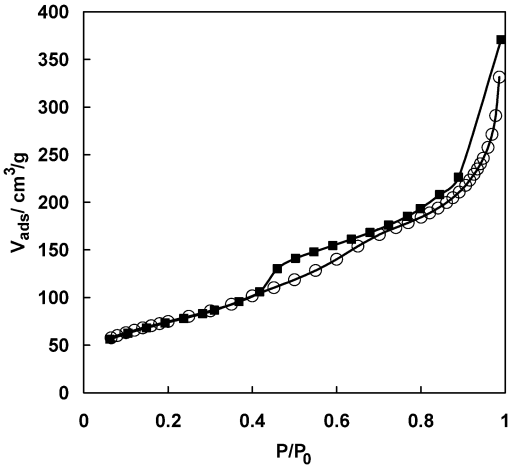

Fig. 5. The adsorption/desorption isotherms of the system obtained with CTAB + TiO_2. (○) Adsorption, (■) desorption.

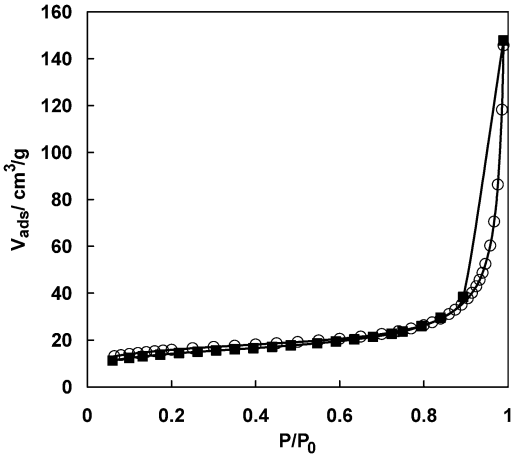

Fig. 6. The adsorption/desorption isotherms of the system obtained with DTAB + TiO_2. (○) Adsorption, (■) desorption.

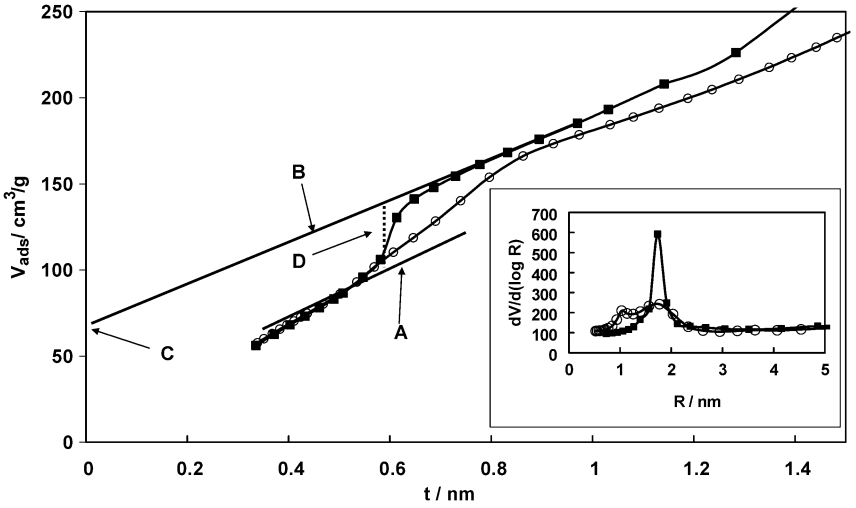

Fig. 7. The t-plot in the system obtained with DTAB + TiO_2. (○) Adsorption, (■) desorption. The explanation of A, B, C and D is in the text. Inset: the pore radius distribution of the CTAB + TiO_2. (○) Adsorption, (■) desorption.

Table 1
Analysis of adsorption results. Nitrogen adsorption data of the different samples

Sample	A_{sp} (m^2/g)	A_{BET} (m^2/g)	A_{tmp} (m^2/g)	A_{text} (m^2/g)	A_{BJHac} (m^2/g)	A_{BJHdc} (m^2/g)	$2l_{molec}$ (nm)	D_{aap} (nm)	D_{aBJH} (nm)	D_{dBJH} (nm)	V_{spat} (cm^3/g)	V_{tpmv} (cm^3/g)	$V_{BJHacvp}$ (cm^3/g)	$V_{BJHdcpv}$ (cm^3/g)
HTAB + TiO_2	260.4529	272.378	7.8476	264.5303	298.4690	319.4861	4.68	6.61121	7.7022	4.3795	0.450187	0.000159	0.574716	0.349801
HTAB		238.6					4.68	4.5522		4.9235	0.44655	0.023219		0.19195
DTAB + TiO_2	55.1219	55.9539	17.2985	38.6554	37.9255	52.1358	3.64	9.54604	23.113	4.9178	0.133534	0.007563	0.219143	0.064098
DTAB	346.4266	369.4441	386.7098	399.7142	386.7098	399.7142	3.64	3.58788	3.4184	3.0859	0.331195	0.03086	0.330481	0.308365
DDAB + TiO_2	41.7530	43.3482	4.0785	39.2696	41.2814	40.8186	3.64	9.67234	20.6634	5.477	0.104820	0.001377	0.213253	0.055891
DDAB	16.8494	17.3252	3.3051	14.0202	17.6757	17.4337	3.64	5.75197	10.1163	4.0112	0.024914	0.001348	0.044703	0.017482

Note. A_{sp}: single point surface area at $p/p_0 = 0.2002$; A_{BET}: BET surface area; A_{tmp}: t-plot micropore area; A_{text}: t-plot external surface area; A_{BJHac}: BJH adsorption cumulative surface area of pores between 3.4 and 600 nm diameter; A_{BJHdc}: desorption cumulative surface area of pores between 3.4 and 600 nm diameter; $2l_{molec}$: twice the length of the surfactant molecule; D_{aap}: adsorption average pore diameter by BET ($8V/A$); D_{aBJH}: BJH adsorption average pore diameter; D_{dBJH}: BJH desorption average pore diameter; V_{spat}: single point adsorption total pore volume of pores; V_{tpmv}: t-plot micropore volume; $V_{BJHacvp}$: BJH adsorption cumulative volume of pores; $V_{BJHdcpv}$: desorption cumulative volume of pores.

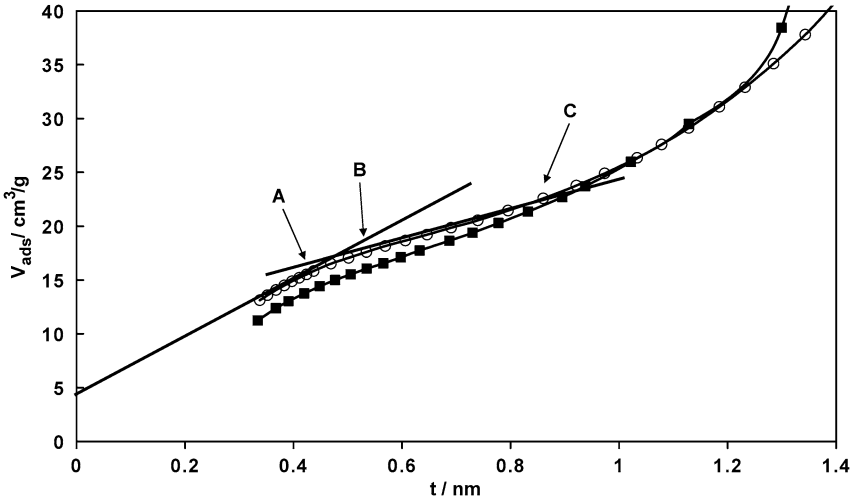

Fig. 8. The t-plot of the DTAB + TiO_2 showing the typical appearance presented by adsorbents with slit-shaped pores). (○) Adsorption, (■) desorption. The explanation of A, B, and C is in the text.

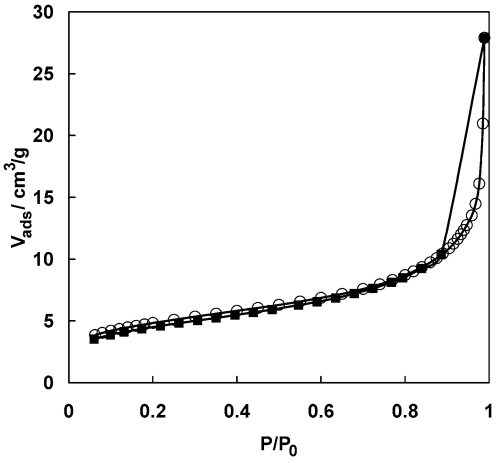

Fig. 9. The adsorption/desorption isotherms of the system obtained with pure DDAB. (○) Adsorption, (■) desorption.

cate an adsorbent with slit-shaped pores as expected, because the template (DDAB) forms a lamellar liquid crystal.

Table 1 summarizes the adsorption results, together with twice the length of the template molecule, which must be similar to the diameter of pores produced by the surfactant microstructures. It may be seen that in general the specific areas of the mesoporous materials here synthesized are low. In literature there are examples of mesoporous materials made with silica including other oxides which have poor specific surface areas, and this area depends on the synthesis conditions [30–32].

To compute the wall thickness, two models were employed. For the lamellar adsorbents a model formed by a parallelepiped weighing one gram and having a total volume of $V_T = 1/\rho_{SiO_2} + V_{pores}$ was considered, where $\rho_{SiO_2} = 2.2$ g/cm^3 is the density of silica. This parallelepiped with height H and section 1 cm^2 is supposed as formed by a pile of $n + 1$ silica lamellae having a thickness h_{SiO_2} intercalated with n slit-shaped pores with average thickness d (Fig. 11A). Then $H = V_T$, $n = V_{pores}/d$, and $h_{SiO_2} = (H - nd)/(n + 1)$. The model for the honeycomb structure is that of Fig. 11B, i.e., a cylinder of adsorbent of hexagonal cross section weighing one gram and having an axial cylindrical pore with average diameter d in the middle and six portions each of 1/3 of a pore, one at each apex, totaling three pores. The length of this body is $L = 4V_{pore}/3\pi d^2$, then the area of the hexagonal face is $A = V_T/L = 6R^2 \tan(\pi/6)$ where R is the length of

Table 2
Computed values of the wall thickness in the different samples

System	CTAB	CTAB + TiO_2	DTAB	DTAB + TiO_2	DDAB	DDAB + TiO_2
Structure	Honeycomb	Honeycomb	Honeycomb	Lamellar?	Lamellar	Lamellar
Wall thickness (nm)	0.91	0.31	0.72	4.31	3.86	4.88

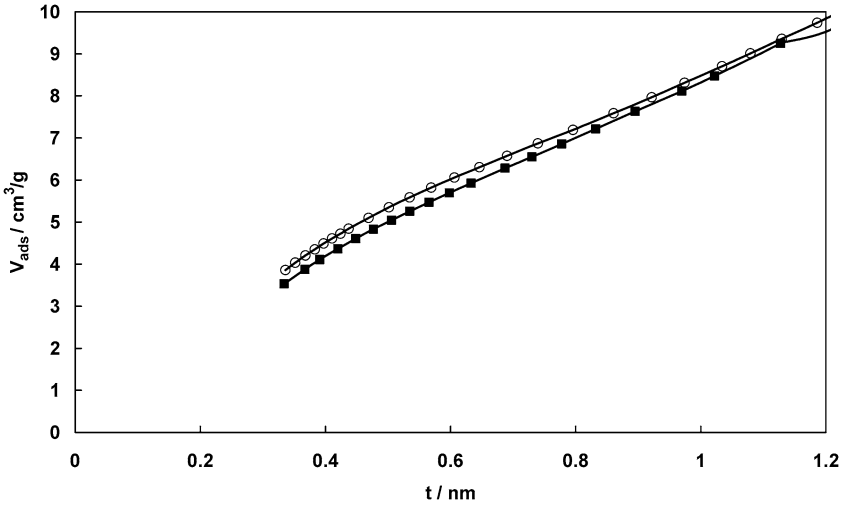

Fig. 10. The t-plot of the system obtained with pure DDAB. (○) Adsorption, (■) desorption.

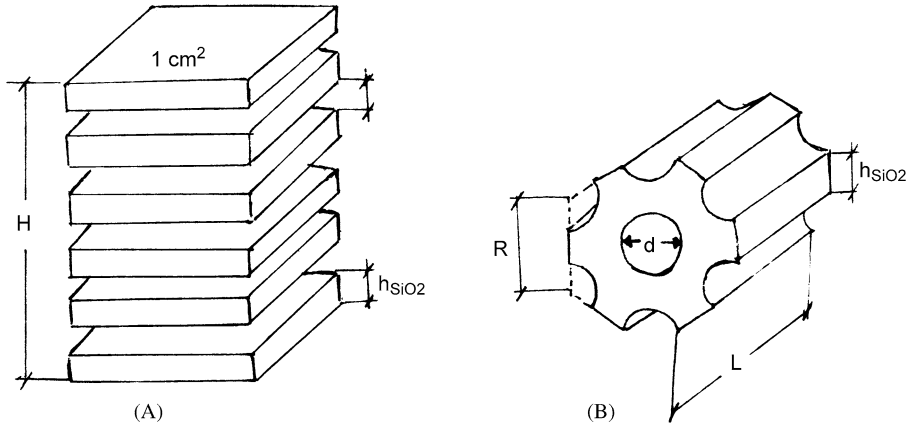

Fig. 11. The models employed to compute the pore walls thickness. A: the model of a lamellar mesoporous material, B: the model for a honeycomb mesoporous material.

one hexagon side. Then $h_{SiO_2} = R - d$. To compute the wall thickness, we used the experimental d values (from Table 1) which were similar to twice the length of the surfactant molecule ($2l_{molec}$). Results are shown in Table 2.

For comparison, highly crystalline silica MCM-41 had $h_{SiO_2} = 1.9$ nm, determined by small X-ray diffraction, but the value obtained by BET adsorption data was 3.8 nm [33,34]. Cheng et al. synthesized silica MCM-41 varying h_{SiO_2} between 1.34 and 2.69 nm simply using different synthesis temperatures (from 70 to 200 °C) and reaction times [35].

4. Discussion and conclusions

The synthesis of titania particles with $TiCl_4$ and AOT/water/n-hexane inverse micelles with $[H_2O]/[AOT] = 10$ gave particles with a diameter 1.7 to 2.9 nm when included in the silica mesoporous material, which is approximately the diameter computed from the initial conditions (3.96 ± 0.03 nm). However, the titania particles obtained by calcination of the microemulsion product were much larger: 13.6 and 18.2 nm. This may mean that calcination produces synterization of the particles, whilst the presence of the silica structures produces separation of the original particles and avoids the synterization. These particles are apparently formed by brookite.

The inclusion of the titania particles in the silica structures produced different results depending on the surfactant employed. In the CTAB templated material the inclusion of the TiO_2 particles produced a moderately BET specific surface area, a 50% increase in the pore average diameter and a reduction in the pore walls thickness, retaining the typical honeycomb structure of MCM-41 materials.

The inclusion of titania in the structures generated by using DTAB produces a different effect. The BET specific surface area was dramatically reduced, while the average pore diameter increased by 200% and the pore wall thickness increased from 0.72 to 4.31 nm. Moreover, the honeycomb structure was transformed into lamellar, as can be seen in the TEM photographs and deduced from the t-plot. The modification of the specific area and the pore diameter and pore wall thickness are also consistent with this structure modification. This may be caused by the difference between the micelle radius of CTAB (4.68 nm, computed as twice the surfactant molecule length) and the DTAB (3.64 nm) cylindrical micelles, when compared with the size of the titania particles covered with AOT (between 3.78 and 4.98 nm), which perturbed the structure of the template. The titania particle fits in the hydrocarbon micelle core of CTAB, but it is too large to fit inside the DTAB micelle core, and this may cause a change in the synthesis which in turn produces the modification of the finally obtained material.

The TiO_2 inclusion in DDAB did not change the lamellar structure, but produced an increase of the BET specific area and the average pore diameter. There was a moderate increase in pore wall thickness. The TEM photographs showed a reduction in the size of the platelets.

Stucky and co-workers [36–42] postulated that due to the dynamic nature of the interaction between inorganic and organic species throughout the synthesis of mesoporous materials, different products would result from a minor change in the mesoporous materials synthesis conditions. The presence of TiO_2 nanoparticles in the reaction media led to a notable perturbation of the synthesis conditions. The mechanism for the production of MCM-41 products suggests that the silicate oligomers initially dissolve into the aqueous regions around surfactant micelles and condensing into layers. At low silicate concentrations, puckering of the silica layers would lead to hexagonal phases, whilst at higher silicate concentration the thicker layers would resist puckering and remains as lamellar phase [39]. In the specific case of our experiments, in addition of silicate there were TiO_2 particles interacting with the surfactant template material. This fact would lead to a more rigid wall surrounding the surfactant micelles, so is it more difficult for the system to pucker and acquire a hexagonal mesophase structure. In the case of DTAB templated material the particles are larger than the micelle diameter and probably modify the mechanism proposed by Stucky et al. On the contrary, the CTAB templated material retained its honeycomb structure because micelles can include the titania particles without a significant change in structure.

Acknowledgments

M.A.M. is a adjunct researcher of the Consejo Nacional de Investigaciones Científicas y Técnicas de la República Argentina (CONICET). P.V.M. is an assistant researcher of the CONICET. M.B.S. has a fellowship of the Comisión de Investigaciones Científicas de la Provincia de Buenos Aires (CIC). This work was financed by a grant of Banco Río and the PIP # 2739 of CONICET.

References

[1] M. Primet, J. Basset, J.V. Mayhieu, M. Prettre, J. Phys. Chem. 74 (1970) 2868.
[2] A. Fujishima, K. Hashimoto, T. Watanabe, TiO_2 Photocatalysis. Fundamentals and Applications, BKC Inc., Tokyo, 1999.
[3] M. Eidenmeyer, S. Grasser, K. Köhler, R. Anwander, Microporous Mesoporous Mater. 44–45 (2001) 3276.
[4] F.-S. Xiao, Y. Han, X. Yu, M. Meng, S. Yang, J. Wu, J. Am. Chem. Soc. 124 (6) (2002) 888.
[5] M. Ogawa, Colloid Polym. Sci. 281 (2003) 665.
[6] J. Mrowiec-Bialon, Polish J. Chem. 74 (2000) 539.
[7] M. Meyer, C.F. Wallsberg, K. Korihara, J.H. Fendler, J. Chem. Soc., Chem. Commun. (1994) 90.
[8] T.F. Towey, A. Khan-Lohdi, B.H. Robinson, J. Chem. Soc., Faraday Trans. 86 (1990) 3757.
[9] L. Motte, C. Petit, L. Boulanger, P. Lixon, M.P. Pileni, Langmuir 8 (1992) 1049.
[10] M.P. Pileni, L. Motte, C. Petit, Chem. Mater. 4 (1992) 338.
[11] T. Hirai, S. Shiojiri, I. Komasawa, J. Chem. Eng. Jpn. 27 (1994) 590.
[12] H. Naono, M. Hakuman, T. Shiono, J. Colloid Interface Sci. 186 (2) (1997) 360.
[13] B.C. Lippens, B.J. Linsen, J.H. Boer, J. Catal. 3 (1964) 32.
[14] K.S.W. Sing, D.H. Everett, R.A.W. Haul, L. Moscou, R.A. Pierotti, J. Rouquérol, T. Semieniewska, Pure Appl. Chem. 57 (4) (1985) 603.
[15] E.P. Barrett, L.G. Joyner, P.H. Halenda, J. Am. Chem. Soc. 73 (1951) 373.
[16] J.H. de Boer, B.C. Lippens, B.G. Linsen, J.C.P. Broekhoff, J. Colloid Interface Sci. 21 (1966) 405.
[17] G. Halsey, J. Chem. Phys. 16 (1948) 931.
[18] A. Zaban, S.T. Aruna, S. Tirosh, B.A. Gregg, Y. Mastai, J. Phys. Chem. B 104 (2000) 4130.
[19] X. Zhao, J. Yu, B. Cheng, Q. Zhang, Colloids Surf. A: Physicochem. Eng. Aspects 268 (2005) 78.
[20] M. Bujan, M. Sikirič, N. Filipovič-Vincekovič, N. Vdovič, N. Garti, H. Füredi-Milhofer, Langmuir 17 (2001) 6461.
[21] G.K. Lim, J. Wang, S.C. Ng, L.M. Gan, Langmuir 15 (1999) 7472.
[22] W.P. Huang, X.H. Tang, Y.Q. Wang, Y. Koltypin, A. Gedanken, Chem. Commun. (2000) 1415.
[23] Y.Q. Zheng, S. Erwei, S.X. Cui, W.J. Li, X.F. Hu, J. Mater. Sci. Lett. 19 (2000) 1445.
[24] C.T. Kresge, M.E. Leonowicz, W.J. Roth, J.S. Beck, Nature 359 (1992) 710.
[25] J.S. Beck, J.C. Vartuli, W.J. Roth, M.E. Leonowicz, C.T. Kresge, K.D. Schmitt, C.T.-W. Chu, D.H. Olson, E.W. Sheppard, S.B. McCullen, J.B. Higgins, J.L. Schlenker, J. Am. Chem. Soc. 114 (1992) 10834.
[26] S.B. McCullen, J.C. Vartuli, J.C. Kresge, W.J. Roth, J.S. Beck, K.D. Scmitt, M.E. Leonowicz, J.L. Schlenker, S.S. Shih, J.D. Lutner, in: T.J. Pinnavaia, M.F. Thorpe (Eds.), Access in Nanoporous Materials, Plenum Press, New York, 1995, p. 1.
[27] C.L. Costa Amaral, R. Itri, M.J. Politi, Langmuir 12 (20) (1996) 4638.
[28] F. Radjy, E.J. Sellevold, J. Colloid Interface Sci. 39 (2) (1972) 367.
[29] E.J. Sellevold, F. Radjy, J. Colloid Interface Sci. 39 (2) (1972) 379.
[30] D.M. Antonelli, J.Y. Ying, Ang. Chem. Int. Ed. Engl. 34 (1995) 2014.
[31] T. Warnheim, A. Jonsson, J. Colloid Interface Sci. 125 (1988) 627.
[32] T. Abe, A. Taguchi, M. Iwamoto, Chem. Mater. 7 (1995) 1429.
[33] A.S. Brown, K.J. Edler, I. Gentle, G.E. Kirton, P.A. Reynolds, P.W. Saville, J. Watson, J.W. White, The Rutherford Appleton Laboratory ISIS facility Annual Report 1996–1997, 1997, p. 52.
[34] K.J. Edler, P.A. Reynolds, J.W. White, D. Cookson, J. Chem. Soc., Faraday Trans. 93 (1997) 199.
[35] C.F. Cheng, W.Z. Zhou, D.H. Park, J. Klinwsky, M. Hargreaves, L.F. Gladuen, J. Chem. Soc., Faraday Trans. 93 (1997) 354.

[36] G.D. Stucky, Q.S. Huo, A. Firouzi, B.F. Chmelka, S. Schacht, I.G. Voigt-Martin, F. Schuth, Stud. Surf. Sci. Catal. 105 (1997) 3.
[37] Q.S. Huo, D.I. Margolese, U. Ciesla, P.Y. Fena, T.E. Gier, P. Sieger, R. Leon, P.M. Petroff, F. Schuth, G.D. Stucky, Nature 36 (1994) 317.
[38] A. Monnier, F. Schuth, Q. Huo, D. Kumar, D. Margolese, R.S. Maxwell, G.D. Stucky, M. Krishnamurty, P. Petroff, A. Firouzi, M. Jamicke, B.F. Chmelka, Science 261 (1993) 1299.
[39] G.D. Stucky, A. Monnier, F. Schuth, Q. Huo, D. Margolese, D. Kumar, M. Krishnamurty, P. Petroff, A. Firouzi, M. Jamicke, B.F. Chmelka, Mol. Cryst. Liq. Cryst. 240 (1994) 187.
[40] U. Ciesla, D. Demuth, R. Leon, P. Petroff, G. Stucky, K. Unger, F. Schuth, J. Chem. Soc., Chem. Commun. (1994) 1387.
[41] Q. Huo, R. Leon, P.M. Petroff, G.D. Stucky, Science 268 (1995) 1324.
[42] V. Alfredsson, M. Keung, A. Monnier, G.D. Stucky, K.K. Unger, F. Schuth, J. Chem. Soc., Chem. Commun. (1994) 921.